Deficiency of *Jamc* Leads to Congenital Nuclear Cataract and Activates the Unfolded Protein Response in Mouse Lenses

Jiani Li, Xuhua Tan, Qihang Sun, Xuri Li, Rongyuan Chen, and Lixia Luo

State Key Laboratory of Ophthalmology, Zhongshan Ophthalmic Center, Sun Yat-sen University, Guangdong Provincial Key Laboratory of Ophthalmology and Visual Science, Guangzhou, China

Correspondence: Rongyuan Chen, Lixia Luo, State Key Laboratory of Ophthalmology, Zhongshan Ophthalmic Center, Sun Yat-sen University, Guangdong Provincial Key Laboratory of Ophthalmology and Visual Science, Jinsui Road No. 7, Guangzhou 510060, China; nullall@163.com, luolixia@mail.sysu.edu.cn.

JL and XT contributed equally to the work presented here and should therefore be regarded as equivalent authors.

PURPOSE. The malfunction of junctional adhesion molecule C (JAM-C) has been reported to induce congenital cataract in humans and mice; however, specific characters and the mechanism of this cataract are still unclear. This study aimed to characterize abnormal lens development in *Jamc* knockout mice and clarify the underlying mechanism.

METHODS. *Jamc* knockout mice backcrossed onto the C57BL/6 genetic background were used for this research. Slit-lamp and darkfield images showed the cataract phenotype of *Jamc*$^{-/-}$ mice. Hematoxylin and eosin staining was performed to visualize the morphological and histological features. RNA sequencing was applied to detect differentially expressed genes. Quantitative RT-PCR, western blot, and immunofluorescence were used to determine the level of unfolded protein response (UPR)-related genes. TUNEL staining was utilized to label cell death.

RESULTS. *Jamc* knockout mice exhibited nuclear cataract with abnormal lens morphology and defective degradation of nuclei and organelles in lens fiber cells. Compared with wild-type control mice, the expression level of BiP, CHOP, TRIB3, and CHAC1, genes involved in endoplasmic reticulum stress and the UPR, were highly upregulated in *Jamc*$^{-/-}$ lenses, suggesting that abnormal lens development was accompanied by UPR activation. Moreover, increased cell death was also found in *Jamc*$^{-/-}$ lenses.

CONCLUSIONS. Congenital nuclear cataract caused by *Jamc* deficiency is accompanied by defective degradation of nuclei and organelles in lens fiber cells, lens structure disorder, and UPR activation, suggesting that JAM-C is required for maintaining normal lens development and that UPR activation is involved in cataract formation in *Jamc*-deficient lenses.

Keywords: JAM-C, congenital cataract, UPR, lens development

The crystalline lens maintains transparency for light transmission, refraction, and accommodation, ensuring that light is focused onto the retina. To facilitate this function, lens development experiences a series of unique and significant processes. The ectoderm-derived lens placode invaginates and forms the lens vesicle, where the anterior cells form the single layer of lens epithelium and posterior cells differentiate into elongated primary lens fiber cells.[1] Lens epithelial cells proliferate and migrate toward the equatorial region and differentiate into secondary lens fiber cells.[2] During the terminal differentiating process, lens fiber cells exit the cell cycle and degrade their subcellular organelles, including nuclei, to finally form an organelle-free zone (OFZ), which is necessary for lens transparency.[3] Any abnormality in the lens development process may cause lens opacity. The opacification of lens present at birth is referred to as congenital cataract, which is the leading cause of blindness in children.[4] Thus, there is an urgent need to elucidate the lens development process and pathological mechanism of congenital cataract. Considering that mutation of some membrane-associated proteins is a common inherited cause of congenital cataract, it is worthwhile to investigate the role of some membrane proteins in lens development.[5]

Junctional adhesion molecule C (JAM-C), a member of the JAM family, contains two extracellular immunoglobulin-like domains: a single transmembrane segment and a relatively short cytoplasmic tail with a PDZ domain–binding motif.[6] As a membrane protein localized to the cell–cell junction, JAM-C has been reported to be involved in inflammation,[7] cell polarity,[8] and tumor metastasis.[9] In addition, it has been reported that JAM-C homozygous mutations exhibited the phenotype of congenital cataracts in several human cases, accompanied with the autosomal-recessive phenotype of hemorrhagic destruction of the brain and subependymal calcification.[10–12] Abnormal retinal structure and congenital cataract were also found in *Jamc* knockout mice.[13] However, the pathological mechanism of congenital cataract induced by malfunction of JAM-C is unclear.

The unfolded protein response (UPR) is an evolutionarily conserved protein quality-control system that maintains cellular homeostasis. Binding immunoglobulin protein (BiP), also known as heat shock protein family A member

5 (HSPA5) or 78-kDa glucose-regulated protein (GRP78), is usually located in the endoplasmic reticulum (ER) membrane and binds to three main UPR sensors (IRE1α, PERK, and ATF6) to keep them inactive.[14] When the accumulation of unfolded, misfolded, or denatured proteins induces ER stress, BiP dissociates from the three sensors and subsequently activates downstream signaling pathways to increase chaperone expression, reduce protein synthesis, and accelerate misfolded protein degradation.[15] Thus, BiP is usually considered to be an ER stress hallmark; however, prolonged ER stress induces cell death when the UPR is insufficient to cope with the stress.[16] Meanwhile, the mediator C/EBP homologous protein (CHOP), also referred to as DNA damage inducible transcript 3 (DDIT3), is upregulated and activated to promote cell apoptosis by inhibiting the transcription of some genes.[17,18] Of note, UPR activation was found in some congenital cataracts, most of which are models of lens-associated genes with aberrant expression, including collagen IV, αA-crystallin, γC-crystallin, connexin 50, and major intrinsic protein (MIP).[19-24] Intense ER stress and UPR-induced apoptosis disrupt lens cellular homeostasis and cause morphologic destruction of the lens. Therefore, we speculated that the cataract caused by *Jamc* deletion may also be associated with UPR activation.

As far as we know, no previous studies have explored congenital cataract in *Jamc* knockout mice. In this study, we aimed to characterize the phenotype of congenital cataract in *Jamc* knockout mice and clarify the possible underlying mechanism. We found retained nuclei and organelles in the presumptive OFZ of *Jamc*$^{-/-}$ lenses and observed lens structure disorder through histology and morphology study. UPR activation and consequent cell death were also found in *Jamc*$^{-/-}$ lenses. Thus, the cataract caused by *Jamc* deficiency may be associated with UPR activation.

MATERIALS AND METHODS

Mice

All animal experiments adhered to the ARVO Statement for the Use of Animals in Ophthalmic and Vision Research and were approved by the animal research ethics committee at the Zhongshan Ophthalmic Center, Sun Yat-sen University. *Jamc* knockout mice, C57bL/6-Jam3$^{tm1.1Chav}$ (http://www.informatics.jax.org/allele/MGI:5140157), were generous gifts from Triantafyllos Chavakis, MD (Technische Universität Dresden, Saxony, Germany).[25] Generation of *Jamc*$^{-/-}$ mice was achieved by intercrossing *Jamc*$^{+/-}$ mice. Embryo ages were timed from the appearance of the vaginal plug (embryonic day 0.5, or E0.5). Genotyping was performed using PCR with the following primer sets: 5′-GCTAGCCTGGTCTATTTAGCCT-3′ and 5′-CCGGACCTGGAGTCGTG-3′. The expected product sizes of *Jamc* wild-type (WT) and knockout are 1000 bp and 400 bp, respectively.

Histological Analysis

Fresh eyeballs or embryonic heads were fixed in FAS Eyeball Fixative Solution (Servicebio, Wuhan, China) and embedded in paraffin. Serial sections were cut at 5-µm thickness through the mid-section of the lens. Slides were stained with hematoxylin and eosin (H&E) and imaged using an upright microscope (ZEISS Axio Imager 2; Carl Zeiss Meditec, Zena, Germany).

Immunofluorescence Staining

For immunofluorescent staining, the eyeballs or embryonic heads were fixed in 4% paraformaldehyde overnight at 4°C and then washed in PBS, followed by incubation in 30% sucrose at 4°C, embedding in optimal cutting temperature (OCT) compound (Crystalgen, Inc., Commack, NY, USA), and subsequent conservation at −80°C. Cryosections were then obtained (10 µm in thickness) and mounted on microscope charged slides. Sections were pretreated for 1 hour in PBS supplemented with 5% donkey serum and 0.5% Triton X-100 at room temperature and then incubated with the primary antibody rabbit anti-BiP (1:200, C50B12; Cell Signaling Technology, Danvers, MA, USA), rabbit anti-TOM20 (1:1000, 11802-1-AP; Proteintech Group, Rosemont, IL, USA), rabbit anti-PDI (1:100, C81H6; Cell Signaling Technology), and rabbit anti-LAMP1 (1:200, ab24170; Abcam, Cambridge, UK) overnight at 4°C and goat anti-JAM-C (1:50, AF1213; R&D Systems, Minneapolis, MN, USA) for 3 hours at room temperature. Invitrogen Alexa Fluor–conjugated secondary antibodies (1:500; Thermo Fisher Scientific, Waltham, MA, USA) were subsequently applied for 1 hour at room temperature. Then, 0.1% 4′,6-diamidino-2-phenylindole (DAPI, 1:1000, D8417; Sigma-Aldrich, St. Louis, MO, USA) was applied for 5 minutes followed by three washes. Sections were imaged using the ZEISS Axio Imager 2 fluorescence microscope.

Western Blot

Lens tissues were ground and lysed in radioimmunoprecipitation assay buffer containing protease and phosphatase inhibitor cocktails (A32961; Thermo Fisher Scientific). Samples were separated on sodium dodecyl sulfate–polyacrylamide gel electrophoresis (SDS-PAGE) gel and transferred to a polyvinylidene difluoride (PVDF) membrane (162-0177; Bio-Rad Laboratories, Hercules, CA, USA). After blocking with 5% non-fat milk, the membrane was incubated with a primary antibody overnight at 4°C, followed by incubation with horseradish peroxidase (HRP)-conjugated secondary antibody (1:5000) for 1 hour at room temperature. The Immobilon Western Chemiluminescent HRP substrate (MilliporeSigma, Burlington, MA, USA) was used to detect specific antibody binding. These signals were captured using a Syngene G:BOX Chemi XT16 imaging device (Syngene, Cambridge, UK). Primary antibodies included goat anti-JAM-C (1:500, AF1189; R&D Systems), rabbit anti-BiP (1:1000, C50B12; Cell Signaling Technology), mouse anti-CHOP (1:1000, sc-7315; Santa Cruz Biotechnology, Dallas, TX, USA), mouse anti-α-tubulin (1:1000, RM2007; Beijing Ray Antibody Biotech, Beijing, China), and mouse anti-β-actin (1:1000, RM2001; RayBiotech).

Real-Time Quantitative PCR

Lens tissues were rinsed with PBS and ground. The total RNA was extracted by TRNzol Universal reagent (DP424; Tiangen Biotech, Beijing, China). cDNA was synthesized using a FastKing RT Kit (Tiangen Biotech) according to the manufacturer's instructions. cDNA was mixed with SYBR Green qPCR Master Mix (Q331-02; Vazyme Biotech, Nanjing, China), and quantitative PCR was performed using an ABI QuantStudio 6 Flex Real-Time PCR System (Life Technologies, Carlsbad, CA, USA). Results were normalized to mouse actin transcripts. The relative fold change in gene expression was calculated using a 2–$\Delta\Delta$Ct method and normalized to

β-actin. Sequences of the primers used for RT-qPCR were as follows:

- Mouse JAM-C exon 1 to exon 5—forward, 5′-TTCCTGCTGCTGCTCTTCAG-3′; reverse, 5′-TCACTGGCTTCACTTGCACA-3′
- Mouse JAM-C exon 4 to exon 7—forward, 5′-ATTGCTTCCAATGACGCAGG -3′; reverse, 5′-ATGCTTCCCTGGGCTCTTATAG-3′
- Mouse BiP—forward, 5′-AGATCTTCTCCACGGCTTCC-3′; reverse, 5′-TGTCTTCAGCTGTCACTCGG-3′
- Mouse CHOP—forward, 5′-AGGAGAACGAGCGGAAAGTG-3′; reverse, 5′-GACCATGCGGTCGATCAGAG-3′
- Mouse TRIB3—forward, 5′-CTGGCTGGCAGATACCCATT-3′; reverse, 5′-TCTGAAGGTTCCTTGCGGAG-3′
- Mouse CHAC1—forward, 5′-GTGGATTTTCGGGTACGGCT-3′; reverse, 5′-ATCTTGTCGCTGCCCCTATG-3′
- Mouse β-actin—forward, 5′-GGAGCAATGATCTTGATCTTC-3′; reverse, 5′-GCCAACACAGTGCTGTCTGG-3′

RNA Sequencing

Total lens RNA from P1, P7, and P21 mice was extracted using the MagZol Reagent (Magen Biotechnology, Guangzhou, China) according to the manufacturer's protocol. Two independent sets of RNA sequencing (RNA-Seq) were carried out. First, RNA from littermate pups ages P1, P7, and P21 ($n = 1$) was used to profile differentially expressed genes over time. Second, three biological replicates of RNA from different P7 littermates were used for validation and to increase the statistical power. The data have been uploaded to the National Center for Biotechnology Information Sequence Read Archive (accession number SRP385054). The quantity and integrity of RNA yield were assessed by using the K5500 microspectrometer (Beijing Kaiao Technology, Beijing, China) and the Agilent 2200 TapeStation (Agilent Technologies, Santa Clara, CA, USA) separately. The libraries were sequenced by Illumina (San Diego, CA, USA) with paired-end 150 bp at RiboBio Co., Ltd. (Guangzhou, China). Differential expression was assessed by DESeq2 using read counts as input. We used the cluster Profiler package in R (R Foundation for Statistical Computing, Vienna, Austria) with Bioconductor and KOBAS 3.0 to identify and visualize the Gene Ontology (GO) terms and Kyoto Encyclopedia of Genes and Genomes (KEGG) pathways enriched by all differentially expressed genes. Differentially expressed genes were chosen according to the criteria of |log2(fold change)| > 1 and adjusted $P < 0.05$. Gene expression differences were compared by reads per kilobase per million mapped reads (RPKM) in the heatmap.

TUNEL Staining

Free 3′-OH DNA double-strand ends were detected using the TUNEL BrightRed Apoptosis Detection Kit (A113-02; Vazyme Biotech) according to the manufacturer's protocol. Briefly, cryosections were digested with proteinase K and then incubated in TdT reaction mix for 1 hour at 37°C. Cell nuclei were stained with 0.1% DAPI. Sections were analyzed using a fluorescence microscope.

Statistical Analysis

All data are represented as means $\pm$ SEM. Prism 8.2.1 (GraphPad Software, San Diego, CA, USA) was used for the statistical analysis. One-way ANOVA followed by Bonferroni's post hoc test was used to compare means among three or more groups. Independent samples *t*-tests were used to compare means between two groups. All statistical tests were two tailed. Values of $P < 0.05$ were considered statistically significant.

RESULTS

Expression of JAM-C in Mouse Lenses

We first detected the expression pattern of JAM-C in different development stages of WT mouse lenses. The mRNA expression level of JAM-C was examined in mouse lenses at stages from early development to adulthood. The results showed similar mRNA expression levels of JAM-C in different stages of WT lenses (Fig. 1B). We subsequently detected JAM-C localization in the lenses through immunofluorescence staining and found that JAM-C was expressed on the lens epithelium layer and the apical end of the fibers in embryonic day (E) 14.5 and P1 lenses (Fig. 1E). In P7 lenses, the expression of JAM-C was detected in cortical fiber cells and lens epithelium (Fig. 1E). Also, clear results by RT-qPCR and western blot showed efficient knockout of JAM-C (Figs. 1C, 1D). Barely positive immunofluorescence signals were detected in lens epithelium or lens fiber cells of P7 *Jamc*$^{-/-}$ lenses, which confirmed the deletion of JAM-C (Fig. 1E).

Congenital Nuclear Cataract in *Jamc* Knockout Mice

Homozygous variants of the *JAMC* gene in human has been reported to be associated with bilateral nuclear cataract at birth.[10-12] The similar phenotype of nuclear cataract was also shown to occur in *Jamc* knockout mice.[26] Slit-lamp photograph showed the phenotype of cataract in *Jamc*$^{-/-}$ mice (Fig. 2A). Darkfield images further indicated the nuclear cataract and smaller lens size in *Jamc*$^{-/-}$ mice (Fig. 2B). Also, by intercrossing *Jamc*$^{+/-}$ mice, the proportion of *Jamc*$^{-/-}$ offspring at postnatal day 7 was only 6.9%, far less than the expected 25% (Fig. 2C). Of note, in the data presented so far, the cataract incidence among *Jamc*$^{-/-}$ mice older than P7 has been 100% (Fig. 2C).

### Lens Developmental Defects in *Jamc*$^{-/-}$ Mice Revealed by Histological Analysis

To further investigate the morphological defects of *Jamc*$^{-/-}$ mouse lenses, H&E staining was used in cross-sections of eyeballs from *Jamc*$^{-/-}$ mice and their control littermates at different stages (Fig. 3). At E14.5, both control and *Jamc*$^{-/-}$ mice exhibited a similar normal differentiation of primary lens fiber cells that had elongated and reached the lens epithelium (Figs. 3A, 3B). At P1, when the OFZ is expected to be formed in WT lenses (Fig. 3C), plenty of nuclei were found in the presumptive OFZ in *Jamc*$^{-/-}$ lenses (Fig. 3D), suggesting that a deficiency of JAM-C causes denucleation disorder. Moreover, severe defects including vacuolization and necrosis were presented in mature lens fiber in P7 *Jamc*$^{-/-}$ lenses (Figs. 3E, 3F), and progressive impairments were found in P14 lenses (Figs. 3G, 3H). Overall, deficiency
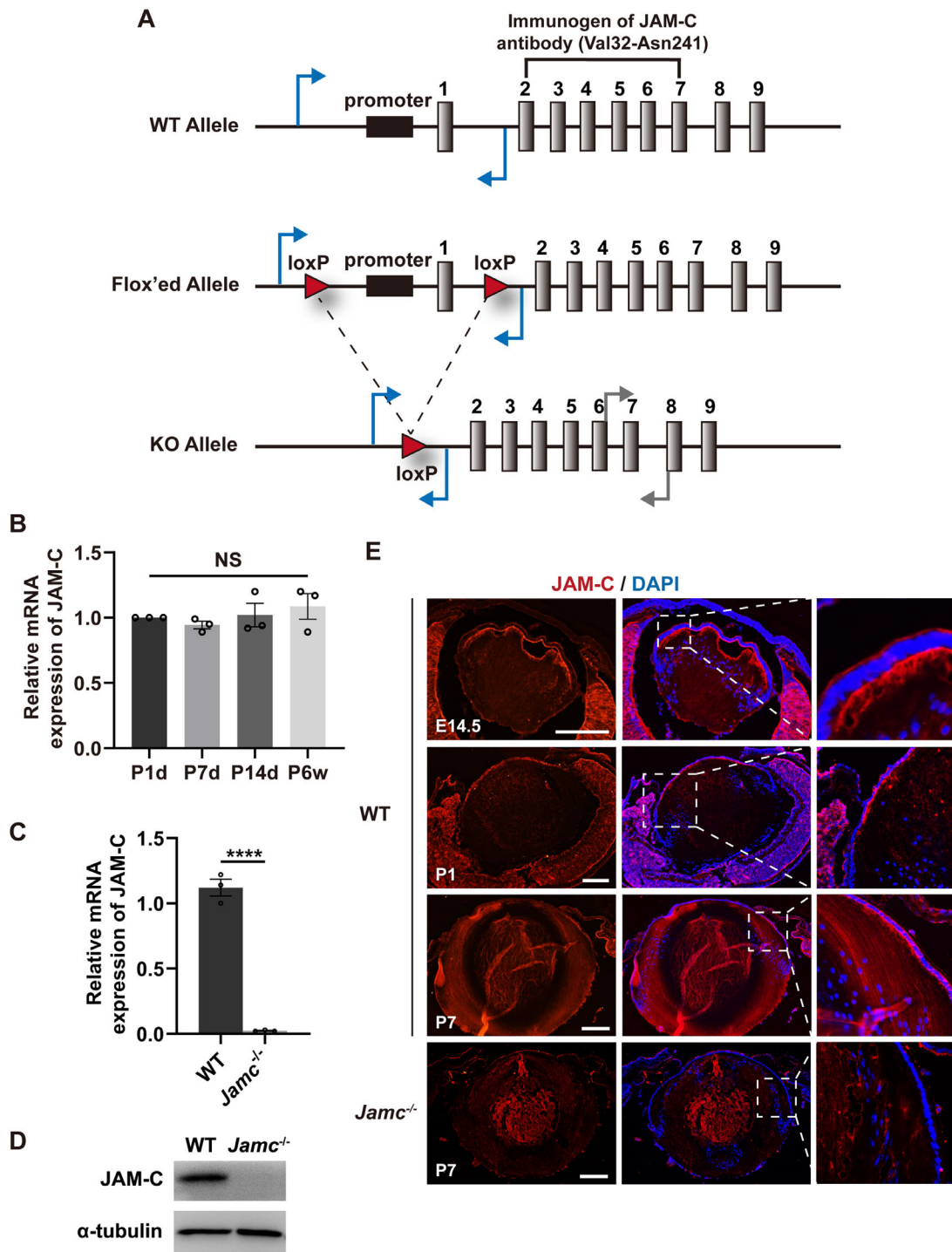
FIGURE 1. JAM-C knockout mice and the expression of JAM-C in WT and *Jamc*$^{-/-}$ mouse lenses. (**A**) Schematic diagram of the generation of JAM-C knockout mice. Two loxP sites (*red triangles*) were inserted to flank the promoter region and exon 1 (*gray box* 1) of *Jamc*. The epitope of the JAM-C antibody corresponds to the coding region between exon 2 and exon 7. Primers used for PCR genotyping are indicated by *blue arrows*. Primers used for qPCR to validate JAM-C deletion are indicated by *gray arrows*. (**B**) Real-time PCR normalized to β-actin revealed that the mRNA expression of JAMC in WT mouse lenses showed no significant differences among the ages of 1 day, 7 days, 14 days, and 6 weeks. The graph is presented as mean ± SEM. NS, not significant; $n = 3$. (**C**) The mRNA expression of JAM-C was determined by real-time PCR, normalized to β-actin in P21 WT and *Jamc*$^{-/-}$ lenses, and then quantified. The mRNA expression of *Jamc* shows a nearly complete knockout in *Jamc*$^{-/-}$ lenses. ****$P < 0.0001$; $n = 3$. (**D**) Proteins were extracted from WT and *Jamc*$^{-/-}$ mice lenses at P14 and then probed for JAM-C expression by western blot; α-tubulin was used as a loading control. The protein expression of JAM-C indicates nearly complete knockout of JAM-C in *Jamc*$^{-/-}$ lenses. (**E**) Representative immunofluorescent staining images of WT and *Jamc*$^{-/-}$ lenses in cryosections for JAM-C (*red*) and DAPI-stained nuclei (*blue*). JAM-C mainly localized on lens epithelium in E14.5 and P1 WT lenses. In P7 WT lenses, JAM-C stains were found in the lens epithelium and cortical lens fiber of WT mice but not in *Jamc*$^{-/-}$ mice. (*Right*) Higher magnifications of boxed areas. *Scale bar*: 200 µm.
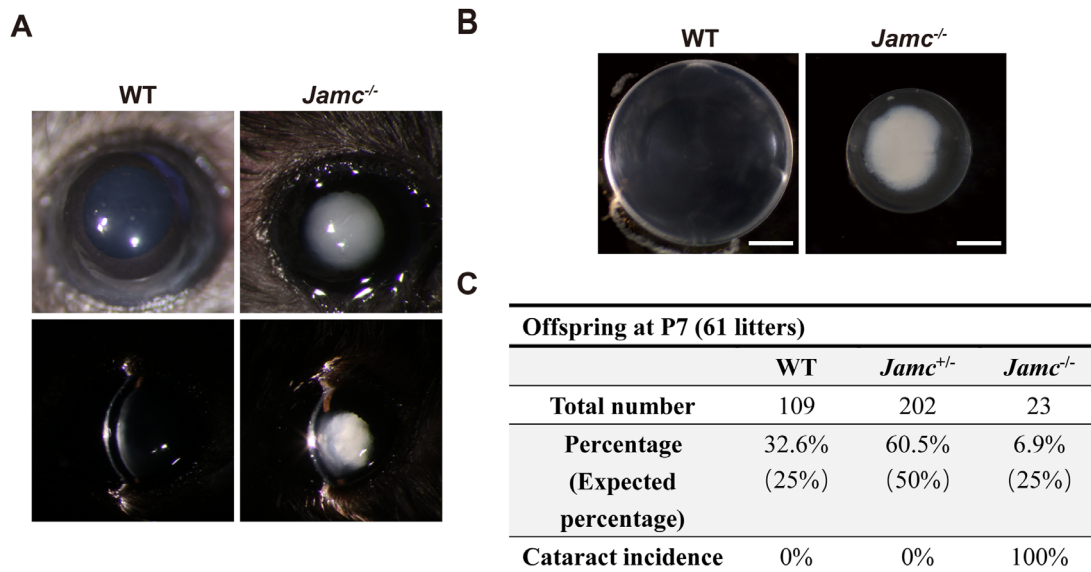
FIGURE 2. Congenital nuclear cataract occurs in *Jamc*$^{-/-}$ mice. (**A**) Slit-lamp view demonstrating transparent lens in WT mice and severe lens opacity in *Jamc*$^{-/-}$ mice (P21). (**B**) Representative darkfield images of lenses in WT and *Jamc*$^{-/-}$ mice (P21) showing nuclear cataract and smaller size in the *Jamc*$^{-/-}$ lenses. *Scale bar*: 500 µm. (**C**) Viability and cataract incidence of offspring (61 litters) at P7. Cataracts were detected with 100% incidence only in *Jamc*$^{-/-}$ mice.

of *Jamc* in the mouse lens results in obvious morphologic destruction during lens development, which would ultimately lead to lens opacity and cataract.

Defective Degradation of Nuclei and Organelles in *Jamc*$^{-/-}$ Mature Lens Fiber Cells

As mentioned before, degradation of nuclei and organelles occurs in terminally differentiated fiber cells. With regard to the failure of denucleation after *Jamc* deletion as observed in H&E staining (Figs. 3C–3H), we speculate that differentiation defects of organelle degradation occurred in *Jamc*$^{-/-}$ mouse lens fiber cells. We used translocase of the outer membrane 20 (TOM20), protein disulfide isomerase (PDI), and lysosome-associated membrane protein 1 (LAMP1) antibodies to visualize the mitochondria, ER, and lysosomes in P1 mice, respectively. In the normal lens, TOM20 expression was located in peripheral cortex fiber cells and absent in the OFZ (Fig. 4A). In contrast, TOM20 and DAPI staining could be observed in the center of *Jamc*$^{-/-}$ lenses, which revealed the failure of denucleation and defective mitochondria degradation in mature fiber cells (Fig. 4B). Similarly, compared with WT control lenses, PDI staining was increased in the presumptive OFZ of *Jamc*$^{-/-}$ lenses (Figs. 4C, 4D). Lysosomes (LAMP1) were also retained in what should be an OFZ in *Jamc*$^{-/-}$ lenses (Figs. 4E, 4F).

Activation of the UPR in *Jamc*$^{-/-}$ Mouse Lenses

To investigate molecular mechanisms of nuclear cataract in *Jamc*$^{-/-}$ mice, lenses from P1, P7, and P21 pups were examined for RNA expression profiling. GO enrichment analysis showed that a set of upregulated genes were enriched in the pathways with regard to *response to endoplasmic reticulum stress* (GO:0034976) and *response to unfolded protein* (GO:0006986) in P21 *Jamc*$^{-/-}$ lenses (Fig. 5A). A similar tendency of those gene sets was found in P1 and P7 groups (Fig. 5A), among which BiP is a master regulator of ER function. Such gene pattern was reproduced in another independent mRNA profiling using lenses from three P7 pups (Supplementary Fig. S1A). Consistently, both mRNA and protein expression levels of BiP were found increased in *Jamc*$^{-/-}$ lenses by independent validation using qPCR and WB (Figs. 5B–5D). Additionally, immunofluorescence staining showed enhanced expression of BiP in P7 *Jamc*$^{-/-}$ lenses (Fig. 5E). Also, the pro-apoptosis protein CHOP was upregulated even in P1 lenses (Figs. 5C, 5D). Moreover, we noted that the mRNA expression levels of tribbles pseudokinase 3 (TRIB3) and glutathione-specific gamma-glutamylcyclotransferase 1 (CHAC1), downstream regulators of CHOP, presented a thousands-fold increase in P21 *Jamc*$^{-/-}$ lenses (Fig. 5B). Collectively, these data show that the UPR was highly activated during developmental stages in *Jamc*$^{-/-}$ lenses accompanied with lens abnormality.

Increased Cell Death in Lens Fiber Cells of *Jamc*$^{-/-}$ Mouse Lenses

Because of the significant upregulation of ER stress-induced pro-apoptosis genes, we speculated that such lens development defects in *Jamc*$^{-/-}$ mice may be accompanied by cell death. Indeed, beyond ER stress-induced pro-apoptosis genes, more genes associated with *cell death* (GO:0008219) and *apoptotic process* (GO:0006915) were upregulated according to GO analysis in *Jamc*$^{-/-}$ P21 lenses (Fig. 6A). Of note, the magnitudes of expression differences for such genes were greater in P21 lenses compared with P1 and P7 lenses, which means the impairment increases with age (Fig. 6A). A similar gene pattern was reproduced in another independent mRNA profiling using lenses from three P7 pups (Supplementary Fig. S1B). We subsequently performed TUNEL staining to identify dying cells in *Jamc*$^{-/-}$ lenses. Stronger and remarkable TUNEL-positive signals were exhibited in deeper mature fiber cells in P7 *Jamc*$^{-/-}$ lenses, indicating the existence of cell death (Fig. 6B).
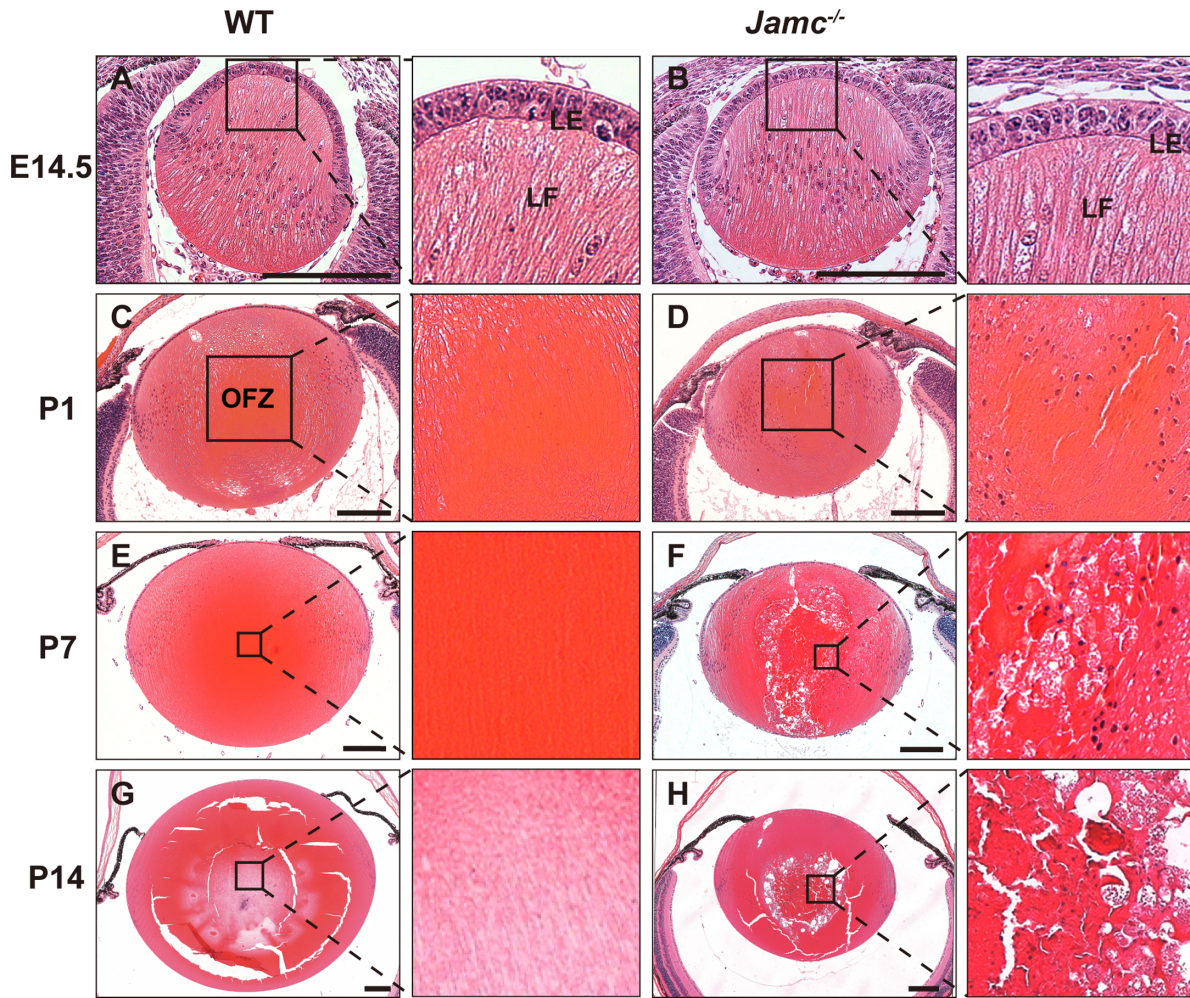
FIGURE 3. Abnormal morphology in $Jamc^{-/-}$ lenses during development. Representative H&E staining images of WT and $Jamc^{-/-}$ lenses in paraffin sections at the ages of E14.5, P1, and P7. (**A**, **B**) Primary lens fiber cells are elongated and have reached the lens epithelium at E14.5. (**C**, **D**) $Jamc^{-/-}$ lens showing the retention of nuclei in the presumptive OFZ and smaller lens size compared with the WT lens at P1. (**E**, **F**) Vacuolization and disordered lens fibers in P7 $Jamc^{-/-}$ lenses. (**G**, **H**) Progressive structural impairment in P14 $Jamc^{-/-}$ lens. LE, lens epithelium; LF, lens fibers. (*Right*) Higher magnifications of boxed areas. *Scale bar*: 200 µm.
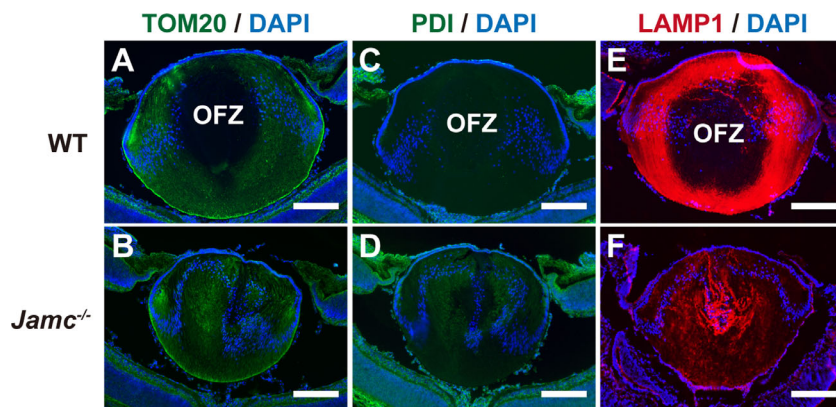
FIGURE 4. Defective degradation of nuclei and organelles in $Jamc^{-/-}$ mature lens fiber cells. Representative immunofluorescent staining images of P1 WT and $Jamc^{-/-}$ lenses in cryosections. TOM20, PDI, and LAMP1 antibodies were used to label mitochondria, ER and lysosomes, respectively. (**A**, **B**) TOM20 staining (*green*) can be observed in the center of the $Jamc^{-/-}$ lens. (**C**, **D**) PDI expression (*green*) located in the presumptive OFZ of the $Jamc^{-/-}$ lens. (**E**, **F**) Decreased LAMP1 (*red*) level and retained LAMP1 staining in the center of the $Jamc^{-/-}$ lens. DAPI-stained nuclei are *blue*. *Scale bar*: 200 µm.
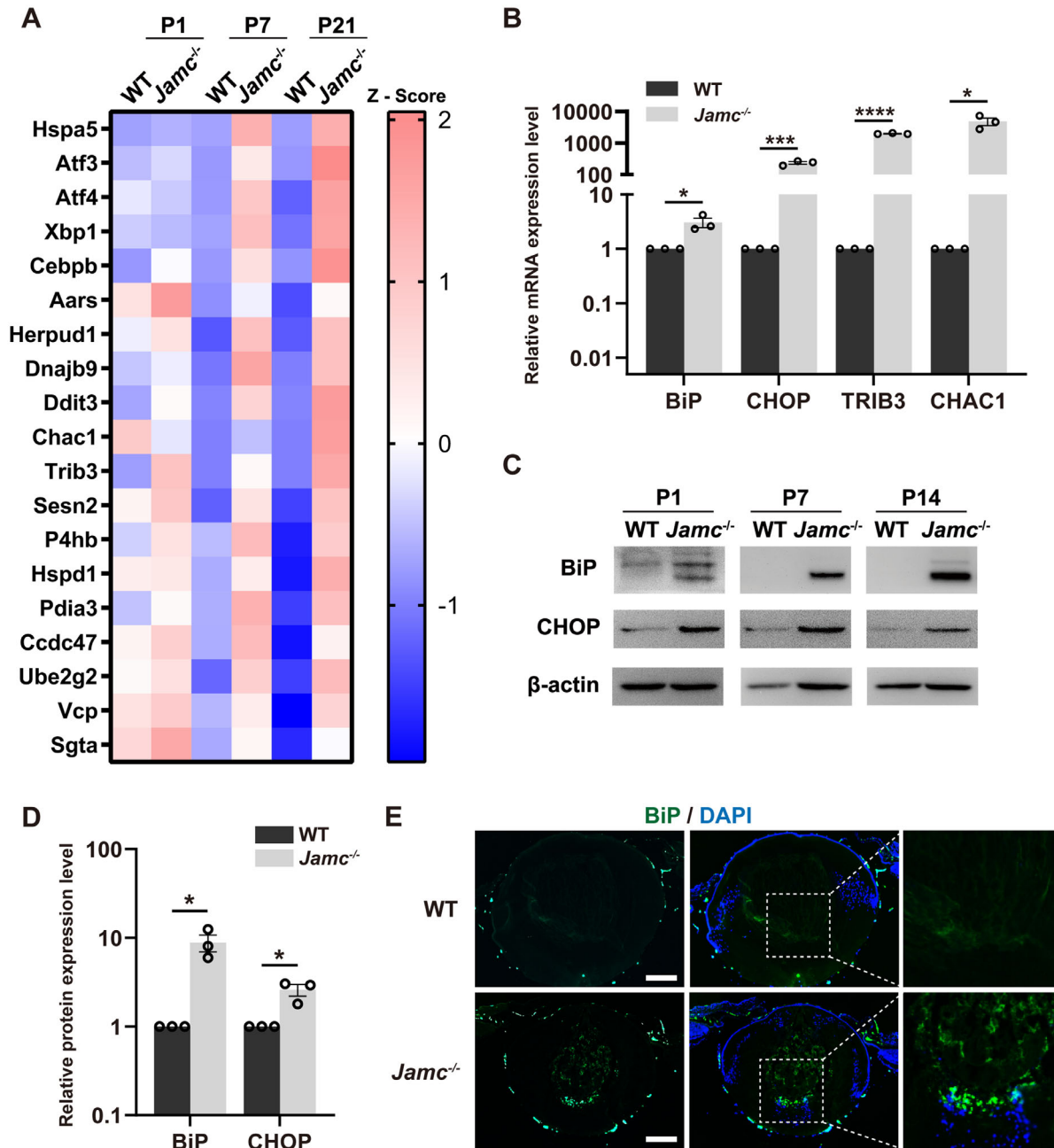
FIGURE 5. UPR activation in $Jamc^{-/-}$ mice lenses. (**A**) Heatmap showing the relative expression value (*z*-score) of 19 genes involved in the response to endoplasmic reticulum stress and unfolded protein response in WT and $Jamc^{-/-}$ lenses at the ages of P1, P7, and P21 according to RNA-Seq data. Genes were obviously upregulated in the P21 $Jamc^{-/-}$ lenses. Similar patterns were also seen in the P1 and P7 groups. (**B**) The mRNA expression of BiP, CHOP, TRIB3, and CHAC1 were determined by real-time PCR and normalized to *β*-actin at P21 and then quantified. These UPR-related genes were significantly upregulated in the $Jamc^{-/-}$ lenses. The graph is presented as mean ± SEM. *$P < 0.05$, ***$P < 0.001$, ****$P < 0.0001$; $n = 3$. NS, not significant. (**C**) The protein expression of BiP and CHOP increased in the $Jamc^{-/-}$ lenses. *β*-actin was used as a loading control. (**D**) Quantification of BiP and CHOP expression levels of the WT and $Jamc^{-/-}$ lenses at P14, as seen in **C**. The fold change relative to the level of control groups is displayed. The protein expression of BiP and CHOP was significantly upregulated in $Jamc^{-/-}$ lenses. The graph is presented as mean ± SEM. *$P < 0.05$; $n = 3$. (**E**) Representative immunofluorescent staining images of P7 WT and $Jamc^{-/-}$ lenses in cryosections for BiP (*green*). DAPI-stained nuclei are *blue*. Increased BiP stains in $Jamc^{-/-}$ lens fiber cells. (*Right*) Higher magnifications of boxed areas. *Scale bar*: 200 µm.

DISCUSSION

JAM-C is usually localized to the most apical region of cell–cell contacts as a tight junction component in epithelial cells.[6] As transmembrane proteins, such as connexins and aquaporin 0, maintain osmosis and metabolite exchange in lenses,[27] JAM-C may play a vital role during lens development. Aberrant JAM-C induces congenital cataracts in both humans and mice, but specific features and underlying mechanisms have not been investigated. In the

A

B
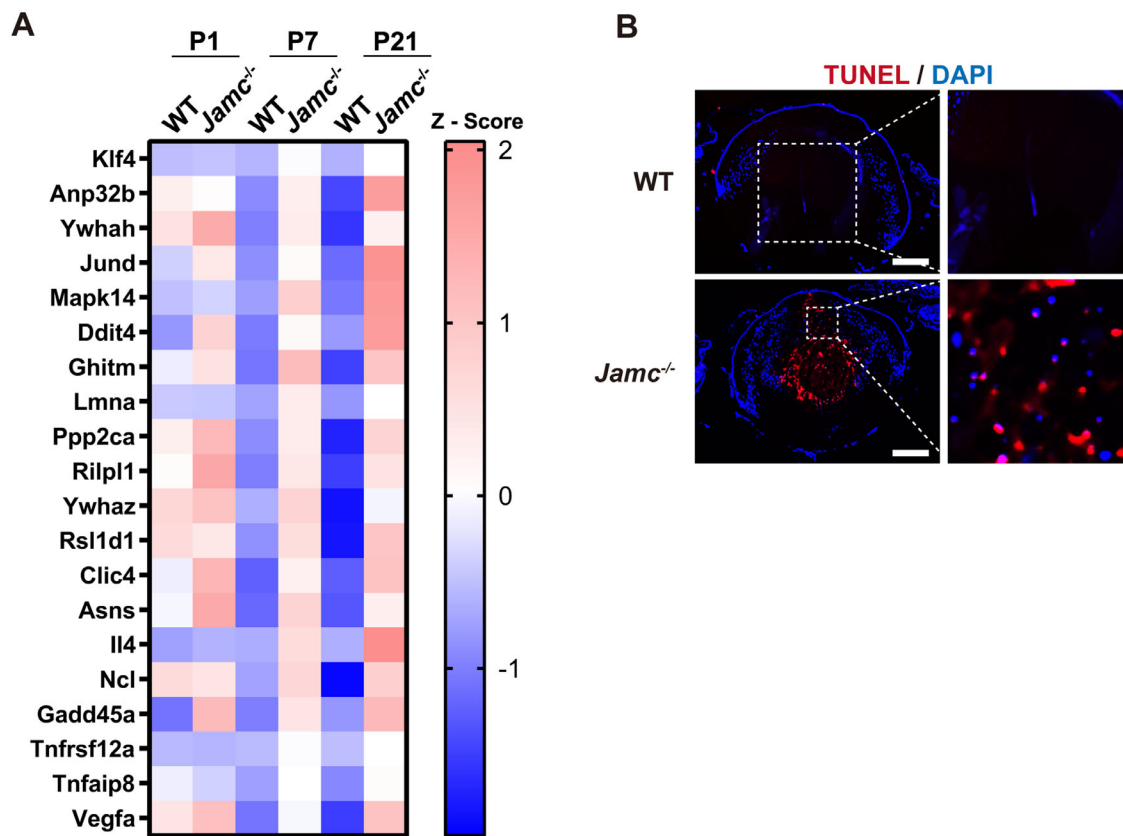
FIGURE 6. JAM-C knockout leads to cell death in mature lens fiber cells. (**A**) Heatmap showing the relative expression value (*z*-score) of 20 genes (UPR-related cell death genes are shown in Fig. 5A) involved in cell death in WT and *Jamc*$^{-/-}$ lenses at the ages of P1, P7, and P21 according to RNA-Seq data. Genes are obviously upregulated in P21 *Jamc*$^{-/-}$ lenses. Similar differentials were also detected in the P1 and P7 groups. (**B**) Representative immunofluorescent staining images of 3'-OH ends of DNA labeled by TUNEL (*red*) in WT and *Jamc*$^{-/-}$ lenses at P7. DAPI-stained nuclei are *blue*. Increased TUNEL-positive staining was detected in *Jamc*$^{-/-}$ lens fiber cells. (*Right*) Higher magnifications of boxed areas. *Scale bar*: 200 µm.

present study, we revealed that UPR activation and UPR-induced cell death may be involved in cataract formation of *Jamc*$^{-/-}$ mice.

Nuclear cataract, a common type of congenital cataract, is often accompanied by the retention of nuclei and organelles in mature lens fiber cells. The elimination of organelles in the central zone of the lens is a unique feature of lens development and differentiation. Nuclei and other organelles degrade when lens epithelial cells differentiate into lens fiber cells and migrate from the equatorial area to the central area, thus minimizing light scatter and ensuring the transparency of the lens.[28] It has been reported that nuclear breakdown is accompanied by the rapid loss of other organelles, including the mitochondria and ER.[29–32] We found an abundance of retained nuclei in the presumptive OFZ of *Jamc*$^{-/-}$ lenses. In addition, abnormal staining of TOM20, PDI, and LAMP1 indicated that the degradation of mitochondria, ER and lysosomes was defective. DNase II-like acid DNase IIβ (DLAD), which is believed to be involved in the degradation of DNA in terminal lens fiber cells, is a lysosomal enzyme.[33] We noted that the LAMP1 expression level was obviously decreased in mouse lenses after *Jamc* deletion (Figs. 4E, 4F). On the other hand, it has been reported that the autophagy–lysosomal pathway is associated with the removal of nuclei and organelles.[34] Therefore, the reduction of LAMP1 staining may explain the defective terminal differentiation of *Jamc*$^{-/-}$ lens fiber cells.

Activation of the UPR has been shown in some congenital cataract models, most of which were induced by mutations of lens-related genes.[19–24] It has been reported that the UPR leads to lens fiber cell differentiation defects, as characterized by attenuated elongation, defective migration, failure of denucleation, and incomplete organelle degradation.[24,35] What's more, prolonged UPR-induced apoptosis in the lens leads to cell death, structural disruption, and vacuolization in some severe situations.[14,23,24,35] Similar phenotypes were also found in *Jamc* knockout lenses, accompanied by UPR activation. We presume that activation of the UPR induces global attenuation of translation, decreases protein synthesis, and results in subsequent initiation of apoptosis, which may disrupt lens homeostasis and finally lead to lens opacity.

The cause of UPR activation in *Jamc* knockout mouse lenses is still unknown. Mutation of genes encoding secreted proteins or membrane proteins such as collagen IV, connexin 50, and MIP may produce unstable mutant proteins that trigger UPR activation. However, our model was based on the deletion of JAM-C, which would not produce such mutant proteins. We subsequently noted several significantly downregulated genes in *Jamc*$^{-/-}$ lenses, such as *Hspb1* and *Hmox1* (data not shown). Because heat shock protein beta-1 (HSPB1) is a modulator of F-actin under stress, reduced HSPB1 expression was thought to be associated with abnormal cellular morphology in the lens.[36] Meanwhile, *hspb1* knockdown in *Xenopus* also causes eye and lens defects.[36]

On the other hand, as a chaperone, the downregulation of HSPB1 itself could be a factor to induce ER stress and UPR activation. More importantly, the *Hmox1* gene encodes heme oxygenase, which plays a protective role against oxidative stress. CHAC1, an enzyme that catalyzes the degradation of glutathione and causes depleted glutathione levels, was found to be significantly upregulated in *Jamc*$^{-/-}$ lenses.[37] Hence, the decrease of *Hmox1* and the increase of CHAC1 after deletion of JAM-C could together support the occurrence of oxidative stress, a well-known inducer of UPR activation. Overall, *Jamc* knockout may activate the UPR by downregulating chaperone gene expression or impairing the capacity to tolerate oxidative stress.

As for the direct cause of *Jamc*-deficient cataract, considering that JAM-C mainly locates in lens epithelium, JAM-C may be critical for maintaining lens epithelial function. Lens epithelial cells play a vital role in keeping lens calcium balance through Ca^{2+}-ATPase.[38] Increased calcium levels in the lens activate the proteolytic enzyme calpain. Calpain-induced proteolysis cleaves various lens proteins, which causes loss of normal lens function and cataract. Calpain activation is a common underlying mechanism for a wide variety of cataracts in rats and mice.[39] Moreover, we also observed that the *cellular response to calcium ion* (GO:0071277) was upregulated according to GO analysis in *Jamc*$^{-/-}$ P7 lenses (data not shown). Therefore, initial damage to the lens epithelium and calpain activation may be the direct cause of cataract formation after JAM-C deletion. In addition, increased calcium disturbs endoplasmic reticulum function, which may also be involved in UPR activation in *Jamc*-deficient mouse lenses.

The cause of UPR activation and the direct cause of cataract in *Jamc*$^{-/-}$ mouse lenses require further investigation. Additionally, the specific molecules or pathways that mediate the UPR and cell death have not yet been identified. More research involving the roles of JAM-C in lens development and its potential role in clinical prediction in cataract will be implemented in the future.

In summary, our research has shown that *Jamc* deletion in mice leads to congenital nuclear cataract, which is characterized by structure disruption and defective differentiation of lens fiber cells. Further study found that the UPR was activated during lens development in *Jamc* knockout mice, suggesting that this cataract may be involved in abnormal UPR activation. Taken together, the finding expanded our knowledge of congenital cataract and revealed that JAM-C plays an indispensable role in homeostasis maintenance in normal lens development.

References

1. Cvekl A, Ashery-Padan R. The cellular and molecular mechanisms of vertebrate lens development. *Development*. 2014;141:4432–4447.
2. Lovicu FJ, McAvoy JW. Growth factor regulation of lens development. *Dev Biol*. 2005;280:1–14.
3. Bassnett S, Mataic D. Chromatin degradation in differentiating fiber cells of the eye lens. *J Cell Biol*. 1997;137:37–49.
4. Khokhar SK, Pillay G, Dhull C, Agarwal E, Mahabir M, Aggarwal P. Pediatric cataract. *Indian J Ophthalmol*. 2017;65:1340–1349.
5. Li J, Chen X, Yan Y, Yao K. Molecular genetics of congenital cataracts. *Exp Eye Res*. 2020;191:107872.
6. Ebnet K. Junctional adhesion molecules (JAMs): cell adhesion receptors with pleiotropic functions in cell physiology and development. *Physiol Rev*. 2017;97:1529–1554.
7. Langer HF, Daub K, Braun G, et al. Platelets recruit human dendritic cells via Mac-1/JAM-C interaction and modulate dendritic cell function in vitro. *Arterioscler Thromb Vasc Biol*. 2007;27:1463–1470.
8. Kim SK, Rulifson EJ. Spermatid differentiation requires the assembly of a cell polarity complex downstream of junctional adhesion molecule-C. *Nature*. 2004;431:316–320.
9. Li X, Yin A, Zhang W, et al. Jam3 promotes migration and suppresses apoptosis of renal carcinoma cell lines. *Int J Mol Med*. 2018;42:2923–2929.
10. Akawi NA, Canpolat FE, White SM, et al. Delineation of the clinical, molecular and cellular aspects of novel *JAM3* mutations underlying the autosomal recessive hemorrhagic destruction of the brain, subependymal calcification, and congenital cataracts. *Hum Mutat*. 2013;34:498–505.
11. Mochida GH, Ganesh VS, Felie JM, et al. A homozygous mutation in the tight-junction protein JAM3 causes hemorrhagic destruction of the brain, subependymal calcification, and congenital cataracts. *Am J Hum Genet*. 2010;87:882–889.
12. De Rose DU, Gallini F, Battaglia DI, et al. A novel homozygous variant in JAM3 gene causing hemorrhagic destruction of the brain, subependymal calcification, and congenital cataracts (HDBSCC) with neonatal onset. *Neurol Sci*. 2021;42:4759–4765.
13. Li Y, Zhang F, Lu W, Li X. Neuronal expression of junctional adhesion molecule-C is essential for retinal thickness and photoreceptor survival. *Curr Mol Med*. 2018;17:497–508.
14. Shiels A, Hejtmancik JF. Inherited cataracts: genetic mechanisms and pathways new and old. *Exp Eye Res*. 2021;209:108662.
15. Hwang J, Qi L. Quality control in the endoplasmic reticulum: crosstalk between ERAD and UPR pathways. *Trends Biochem Sci*. 2018;43:593–605.
16. Lai E, Teodoro T, Volchuk A. Endoplasmic reticulum stress: signaling the unfolded protein response. *Physiology (Bethesda)*. 2007;22:193–201.
17. Tabas I, Ron D. Integrating the mechanisms of apoptosis induced by endoplasmic reticulum stress. *Nat Cell Biol*. 2011;13:184–190.
18. Rasheva VI, Domingos PM. Cellular responses to endoplasmic reticulum stress and apoptosis. *Apoptosis*. 2009;14:996–1007.
19. Firtina Z, Danysh BP, Bai X, Gould DB, Kobayashi T, Duncan MK. Abnormal expression of collagen IV in lens activates unfolded protein response resulting in cataract. *J Biol Chem*. 2009;284:35872–35884.
20. Andley UP, Goldman JW. Autophagy and UPR in alpha-crystallin mutant knock-in mouse models of hereditary cataracts. *Biochim Biophys Acta*. 2016;1860:234–239.
21. Ma Z, Yao W, Theendakara V, Chan CC, Wawrousek E, Hejtmancik JF. Overexpression of human γC-crystallin 5 bp duplication disrupts lens morphology in transgenic mice. *Invest Ophthalmol Vis Sci*. 2011;52:5369–5375.
22. Alapure BV, Stull JK, Firtina Z, Duncan MK. The unfolded protein response is activated in connexin 50 mutant mouse lenses. *Exp Eye Res*. 2012;102:28–37.
23. Zhou Y, Bennett TM, Shiels A. Lens ER-stress response during cataract development in Mip-mutant mice. *Biochim Biophys Acta*. 2016;1862:1433–1442.
24. Reneker LW, Chen H, Overbeek PA. Activation of unfolded protein response in transgenic mouse lenses. *Invest Ophthalmol Vis Sci*. 2011;52:2100–2108.

25. Langer HF, Orlova VV, Xie C, et al. A novel function of junctional adhesion molecule-C in mediating melanoma cell metastasis. *Cancer Res*. 2011;71:4096–4105.

26. Daniele LL, Adams RH, Durante DE, Pugh EN, Jr, Philp NJ. Novel distribution of junctional adhesion molecule-C in the neural retina and retinal pigment epithelium. *J Comp Neurol*. 2007;505:166–176.

27. Jiang JX. Gap junctions or hemichannel-dependent and independent roles of connexins in cataractogenesis and lens development. *Curr Mol Med*. 2010;10:851–863.

28. Bassnett S. On the mechanism of organelle degradation in the vertebrate lens. *Exp Eye Res*. 2009;88:133–139.

29. Bassnett S. Mitochondrial dynamics in differentiating fiber cells of the mammalian lens. *Curr Eye Res*. 1992;11:1227–1232.

30. Bassnett S, Beebe DC. Coincident loss of mitochondria and nuclei during lens fiber cell differentiation. *Dev Dyn*. 1992;194:85–93.

31. Dahm R, Gribbon C, Quinlan RA, Prescott AR. Changes in the nucleolar and coiled body compartments precede lamina and chromatin reorganization during fibre cell denucleation in the bovine lens. *Eur J Cell Biol*. 1998;75:237–246.

32. Bassnett S. The fate of the Golgi apparatus and the endoplasmic reticulum during lens fiber cell differentiation. *Invest Ophthalmol Vis Sci*. 1995;36:1793–1803.

33. Nishimoto S, Kawane K, Watanabe-Fukunaga R, et al. Nuclear cataract caused by a lack of DNA degradation in the mouse eye lens. *Nature*. 2003;424:1071–1074.

34. Basu S, Rajakaruna S, Reyes B, Van Bockstaele E, Menko AS. Suppression of MAPK/JNK-MTORC1 signaling leads to premature loss of organelles and nuclei by autophagy during terminal differentiation of lens fiber cells. *Autophagy*. 2014;10:1193–1211.

35. Ma Z, Yao W, Chan CC, Kannabiran C, Wawrousek E, Hejtmancik JF. Human βA3/A1-crystallin splicing mutation causes cataracts by activating the unfolded protein response and inducing apoptosis in differentiating lens fiber cells. *Biochim Biophys Acta*. 2016;1862:1214–1227.

36. Barnum CE, Al Saai S, Patel SD, et al. The Tudor-domain protein TDRD7, mutated in congenital cataract, controls the heat shock protein HSPB1 (HSP27) and lens fiber cell morphology. *Hum Mol Genet*. 2020;29:2076–2097.

37. Kumar A, Tikoo S, Maity S, et al. Mammalian proapoptotic factor ChaC1 and its homologues function as γ-glutamyl cyclotransferases acting specifically on glutathione. *EMBO Rep*. 2012;13:1095–1101.

38. Rhodes JD, Sanderson J. The mechanisms of calcium homeostasis and signalling in the lens. *Exp Eye Res*. 2009;88:226–234.

39. Shearer TR, Ma H, Fukiage C, Azuma M. Selenite nuclear cataract: review of the model. *Mol Vis*. 1997;3:8.